

# Driving large-velocity propagation of ferromagnetic $\pi/2$ domain walls in nanostripes of cubic-anisotropy materials

Andrzej Janutka<sup>†</sup>, Przemysław Gawroński<sup>‡</sup> and Paweł S Ruszala<sup>§</sup>

<sup>†</sup> Department of Theoretical Physics, Wrocław University of Technology, 50-370 Wrocław, Poland

<sup>‡</sup> Faculty of Physics and Applied Computer Science, AGH University of Science and Technology, 30-059 Krakow, Poland

<sup>§</sup> Faculty of Fundamental Problems of Technology, Wrocław University of Technology, 50-370 Wrocław, Poland

**Abstract.** We study the externally-driven motion of the domain walls (DWs) of the  $\pi/2$  type in (in-the-plane ordered) nanostripes with the crystalline cubic anisotropy. Such DWs are much narrower than the transverse and vortex  $\pi$  DWs in the soft-magnetic nanostripes while they propagate much faster, thus, enabling dense packing of magnetization domains and high speed processing of the many-domain states. The viscous current-driven motion of the DW with the velocity above 1000m/s under the electric current of the density  $\sim 10^{12}$  A/m<sup>2</sup> is predicted to take place in the nanostripes of the magnetite. Also, the viscous motion with the velocity above 700m/s can be driven by the magnetic field according to our solution to a 1D analytical model and the micromagnetic simulations. Such huge velocities are achievable in the nanostripes of very small cross-sections (only 100nm width and 10nm thickness). The fully stress driven propagation of the DW in the nanostripes of cubic magnetostrictive materials is predicted as well. The strength of the DW pinning to the stripe notches and the thermal stability of the magnetization during the current flow are addressed.

PACS numbers: 75.78.Cd, 75.78.Fg, 85.70.Ec, 85.70.Kh

E-mail: Andrzej.Janutka@pwr.edu.pl

## 1. Introduction

The domain walls (DWs) in the ferromagnetic nanowires (nanostripes) are the objects of a huge current interest because of concepts of miniaturization of the non-volatile memory and of the magnetics-based logic. Especially, the idea of the 3D digital recording known as the "domain-wall racetrack memory" has taken enormous attention of the magnetics community [1, 2]. It is based on positioning a train of the magnetic DWs in the nanowire with the electric current. However, the racetrack concept has met difficulties. The most challenging of them is claimed to be a rapid increase of the temperature during the current-driven propagation of the DWs (a fast Joule heating) [3, 4]. The minimum value of the spin transfer torque (STT), thus, the minimum intensity of the applied current and the minimum pace of the Joule heating are limited by two factors. These are the DW pinning to natural and artificial (position-stabilizing) defects of the stripe and the need for reducing the operating time via increasing the DW velocity. Overcoming this difficulty has motivated the evolution of the DW racetrack architecture whose primary step was usage of the nanostripes with perpendicular magnetic anisotropy (PMA) instead of the longitudinally magnetized stripes [5]. However, since the PMA stripes are the uniaxial ferromagnets in principle, the field and current driven motions of the DW are turbulent whereas the record stability requires them to be viscous [6, 7]. By the viscous motion we mean a uniform translational movement without the magnetization precession in the transverse plane (it takes place below the Walker breakdown). This requirement is satisfied in double-layer (or triple-layer) nanowires composed of a PMA ferromagnet (ferromagnets) and a non-magnetic metal. The stable (uniform) and fast current-driven propagation of the DW stack is possible utilizing the spin-Hall effect in the non-magnetic layer provided the global chirality of the DW system is stabilized by an interface-induced (Dzyaloshinskii-Moriya-like) anisotropy [8].

Simplifying the racetrack architecture is of importance with regard to the purpose of manufacturing the 3D memory device. The challenge is the stabilization of the DW structure in a simple nanowire (a single-layer nanostripe), thus, shifting the Walker-breakdown point upward the axis of the magnetic-field intensity. Our hypothesis is that the presence of two easy (or two hard) anisotropy axes could improve the stability. In particular, the racetrack created of a ferromagnetic material with a multi-axis crystalline anisotropy is an option to consider. Small width and high mobility of the DWs are desired and these advantages determine our preferences in terms of the material and sizes of the nanostripe.

In a recent paper, analyzing the structure of the ferromagnetic DWs in the nanostripes made of cubic anisotropy materials, we (A.J. and P.G.) have predicted the  $\pi/2$  DW to stabilize in sufficiently-thin stripes (e.g. of  $\text{Fe}_3\text{O}_4$ ) provided the stripe axes coincide with the hard directions of the crystalline anisotropy [9]. Those DWs separate the domains magnetized along the easy axes in the stripe plane (diagonal to the stripe axes). Such an ordering requires the saturation magnetization to be small enough that the magnetostatic (shape-anisotropy) energy  $E_{ms} = -\mu_0 \int \mathbf{m} \cdot \mathbf{H}_d(\mathbf{m}) dV$  is comparable to the exchange energy  $E_{ex} = A \int \sum_{i=x,y,z} |\nabla m_i|^2 dV$  and it does not exceed the energy of the crystalline anisotropy  $E_{an} \approx K_1/M^4 \int m_x^2 m_y^2 dV$  (written up to the leading term). Here  $\mathbf{m}$  denotes the magnetization, ( $M \equiv |\mathbf{m}|$  and  $z$  axis is normal to the stripe plane),  $\mathbf{H}_d$  denotes the dipole field,  $A$  and  $K_1 < 0$  are the exchange stiffness and cubic-anisotropy constant, respectively. In the static case, the cubic anisotropy is equivalent to the four-fold in-the-plane anisotropy due to the

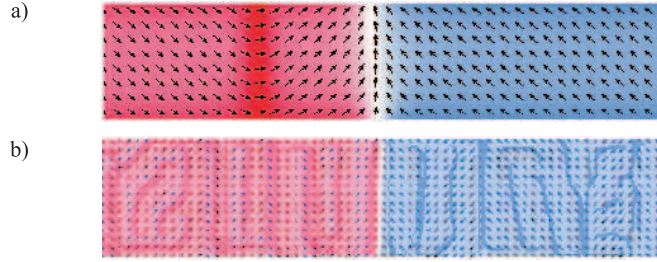


**Figure 1.** A static  $\pi/2$  head-to-head DW in the neighborhood of a head-to-tail  $\pi/2$  DW in: a  $w \times \tau = 400 \times 10\text{nm}^2$  cross-section nanostripe of the magnetite (a), and a static  $\pi/2$  head-to-head DW in the neighborhood of many head-to-tail DWs in a  $w \times \tau = 400 \times 40\text{nm}^2$  cross-section nanostripe of the Terfenol-D (b). The colors and their intensity indicate the sign and value of the projection of the magnetization on the long axis of the stripe.

planar alignment of the magnetization. The width of the  $\pi/2$  DWs has appeared to be independent of the stripe width and much smaller than the width of the transverse or vortex DWs in soft-ferromagnetic nanostripes or in thicker nanostripes of the cubic materials as well. The small width of the  $\pi/2$  DWs is expected to enable packing the bits (domains) in the racetrack with a density comparable to that in the PMA nanostripes.

The aim of the present paper is to study the field-driven, current-driven, and stress-driven dynamics of the head-to-head (tail-to-tail)  $\pi/2$  DWs in the nanostripes made of cubic-anisotropy ferromagnet with regard to the racetrack design. We estimate the velocities of the DW under different external drivings. The strength of pinning of the  $\pi/2$  DW to a notch at one of the stripe edges is examined and the depinning current is determined. For the minimum current intensity established, the pace of the temperature increase due to the Joule heating is evaluated. Hence, we determine the main limitations of the  $\pi/2$ -DW based racetracks.

The recent rapidly increasing interest in the methods of control of the magnetization state via the stress application (the straintronics) is motivated by the hope for reducing the energy consumption compared to the application of the magnetic field or the electric current. The strong crystalline anisotropy, in particular, the cubic anisotropy, is often accompanied by a significant magnetostriction [10]. This is shown below to offer a possibility of driving the head-to-head (tail-to-tail)  $\pi/2$  DW propagation via the application of the mechanical stress. The study of the efficiency of such a driven motion completes the present analysis of the potential of the  $\pi/2$  DW for the racetracks.

In sec. II, we provide a background of the  $\pi/2$  DWs in the cubic-anisotropy materials and consider the ways of driving the DW propagation. The field and current driven motions of the  $\pi/2$  DWs in the nanostripe are investigated in subsec. IIIa, while the depinning from the notch is studied in subsec. IIIb. Sec. IV is devoted to analyzing the stress-driven motion of the  $\pi/2$  DW. Conclusions are collected in sec. V.

## 2. Background

In the previous work, we have performed the micromagnetic simulations of the DW formation in the nanostripes made of cubic-anisotropy materials and we have

developed an analytical description of the DW structures [9]. The density of the crystalline-anisotropy energy of the relevant cubic ferromagnets takes the form

$$\mathcal{H}_a = \frac{K_1}{M^4} (m_x^2 m_y^2 + m_y^2 m_z^2 + m_z^2 m_x^2) + \frac{K_2}{M^6} m_x^2 m_y^2 m_z^2, \quad (1)$$

see e.g. [10]. For a certain range of the material parameters (when the exchange lengths  $l_{ex} = \sqrt{2A/\mu_0 M^2}$ ,  $l_K = \sqrt{-A/K_1}$  are comparable), in very thin nanostripes [of the thickness of the order of  $l_{ex}^2/l_K$ ], the  $\pi/2$  DWs are stable solutions to the Landau-Lifshitz-Gilbert equation. In particular, they have been found with the material constants of the magnetite ( $\text{Fe}_3\text{O}_4$ ) for the nanostripe thicknesses of up to 20nm and with the parameters of the Terfenol-D ( $\text{Tb}_{0.3}\text{Dy}_{0.7}\text{Fe}_2$ ) for the nanostripe thicknesses of up to 50nm, in the case of the crystallographic axes aligned parallel to the relevant stripe axes. The following material parameters of  $\text{Fe}_3\text{O}_4$  have been included:  $M = 3 \cdot 10^5 \text{A/m}$ ,  $K_1 = -1.1 \cdot 10^4 \text{J/m}^3$ ,  $K_2 = -0.3 \cdot 10^4 \text{J/m}^3$ ,  $A = 1.2 \cdot 10^{-11} \text{J/m}$ , the Gilbert damping constant  $\alpha = 0.014$ , and the gyromagnetic ratio  $\gamma \approx \mu_0^{-1} \cdot 2.21 \cdot 10^5 \text{m/As}$ , [11, 12, 13, 14]. We remark that the effective saturation magnetization for the film of the magnetite is significantly smaller than for the bulk material ( $M = 4.8 \cdot 10^5 \text{A/m}$ ), which is due to the presence of anti-phase areas [13]. The mechanism of the anti-phase appearance is connected to an antiferromagnetic interaction at the anti-phase boundaries [15]. It is local and not expected to influence the energy of the single-ion anisotropy, thus, we use the anisotropy constants of the bulk. Let us mention that, contrary to previous reports on the attenuation of the anisotropy in the  $\text{Fe}_3\text{O}_4$  films, careful analysis suggests the four-fold in-the-plane anisotropy of the thin layers of the magnetite to be even stronger than in the thick films (the bulk limit) [16]. The relevant parameters of  $\text{Tb}_{0.3}\text{Dy}_{0.7}\text{Fe}_2$  are following:  $M = 7.5 \cdot 10^5 \text{A/m}$ ,  $K_1 = -8.7 \cdot 10^5 \text{J/m}^3$ ,  $K_2 = 2.3 \cdot 10^6 \text{J/m}^3$ ,  $A = 9.0 \cdot 10^{-12} \text{J/m}$ ,  $\alpha = 0.1$ , [17, 18].

The presence of the  $\pi/2$  DWs is a consequence of a large in-the-plane tilt of the direction of the domain magnetization from the long axis of the stripe, (see figure 1), that results from the strong crystalline anisotropy (in the case  $K_1 < 0$ ). The competition between the crystalline and shape anisotropies (the effect of the demagnetization field) results in a limitation on the length of the uniformly magnetized domains, thus, it leads to the creation of periodic structures of head-to-tail  $\pi/2$  DWs in the nanostripe (modulated superdomains). The superdomains of different projections of the magnetization onto the long axis of the stripe are separated by head-to-head or tail-to-tail  $\pi/2$  DWs, (similar structures of  $\pi/2$  DWs are observed in nm-thickness rings of  $\text{Fe}_3\text{O}_4$ , [19]). Hence, unlike in the proposals of the  $\pi$ -DW racetrack, we consider a record of bits which are written in patterned superdomains. The period of the patterns depends on the saturation magnetization (on the ratio  $\mu_0 M^2/K_1$ , where  $\mu_0$  denotes the vacuum permeability) and on the thickness of the stripe since these two factors influence the demagnetization (dipole) field.

Similar to case of the  $\pi$  DWs in the stripes and wires, the uniform electric current through the cubic-anisotropy nanostripe induces STT in the DWs driving the propagation of all  $\pi/2$  DWs through the nanostripe in the same direction. Also, similar to the case of the  $\pi$  DWs, the application of an external longitudinal magnetic field drives the neighboring head-to-head and tail-to-tail  $\pi/2$  DWs to propagate in the opposite directions because the superdomains magnetized parallel (antiparallel) to the field must expand (shrink) [20].

Another way of driving the motion of the DW can arise when the neighboring ferromagnetic domains are not magnetized parallel to each other as it is in the

nanostripes under consideration. Any uniform in-the-plane stress applied in a different direction than the stripe axes is expected to induce a difference of the anisotropy energies of the neighboring domains due to the magnetostriction, thus, to drive expansion or shrinking of the domains [21, 22]. In the case of a pair of one head-to-head and one tail-to-tail DWs magnetized in the same direction (of the opposite chiralities), the application of such a stress is expected to result in the mutual collision of the DWs and, provided the DW motion was viscous, in their annihilation. Hence, the stress application is a potential alternative to usage of the external magnetic field, in particular, with the purpose of manipulating the bit record via the annihilation of the DW pairs (the reversal of the superdomain magnetization).

Because of the above, materials of strong (giant) magnetostriction are of our especial interest. Within the class of them, besides the magnetite and Terfenol-D, we have managed to simulate the  $\pi/2$  DWs in thin nanostripes of the cobalt ferrite ( $\text{CoFe}_2\text{O}_4$ ). Remark that the nanotechnology of the Terfenol-D remains a challenge however. Unfortunately, simulating the domain wall creation in the nanostripes of the cubic-anisotropy and high-magnetostriction  $\text{Fe}_{1-x}\text{Ga}_x$  (Galfenol-like) alloys (of the 10nm thickness at least), we have not managed to find the  $\pi/2$  DWs for any concentration  $x$ . This fact resembles quite high ratio of the exchange length of the crystalline anisotropy to the magnetostatic exchange length for  $\text{Fe}_{1-x}\text{Ga}_x$ , [9].

The density of the magnetoelastic energy of the cubic ferromagnet is of the form

$$\mathcal{H}_{me} = -\frac{3}{2M^2|\sigma|}\lambda_{100}(m_x^2\sigma_x^2 + m_y^2\sigma_y^2 + m_z^2\sigma_z^2) - \frac{3}{M^2|\sigma|}\lambda_{111}(m_xm_y\sigma_x\sigma_y + m_xm_z\sigma_x\sigma_z + m_y m_z\sigma_y\sigma_z), \quad (2)$$

where  $\sigma$  denotes the stress vector, and  $M \equiv |\mathbf{m}|$  is the saturation magnetization [10]. Applied to the cubic media, one uses the name 'giant magnetostriction' referring to the materials of large value of the volume magnetostriction parameter;  $\lambda = 2/5\lambda_{100} + 3/5\lambda_{111}$ , where  $\lambda_{100}$ ,  $\lambda_{111}$  determine the tetragonal and rhombohedral magnetostrictions respectively. The last formula holds for the polycrystalline ferromagnets [23]. When inducing the DW translation in a single-crystal film using the stress, the strong rhombohedral magnetostriction is needed. The energy of the tetragonal magnetostriction of the neighboring domains is independent on whether they are magnetized parallel or not provided the absolute values of the angles between the domain magnetization and the stripe axes are globally conserved. The energy of the rhombohedral magnetostriction makes a difference. Moreover, large value of the ratio  $\lambda_{111}/\lambda_{100}$  is an advantage (see Appendix B). Therefore, the materials of strong rhombohedral magnetostriction:  $\text{Fe}_3\text{O}_4$ , ( $\lambda_{100} = -19 \cdot 10^{-6}$  and  $\lambda_{111} = 81 \cdot 10^{-6}$ );  $\text{CoFe}_2\text{O}_4$ ; ( $\lambda_{100} = -590 \cdot 10^{-6}$  and  $\lambda_{111} = 120 \cdot 10^{-6}$ ) [12];  $\text{Tb}_{0.3}\text{Dy}_{0.7}\text{Fe}_2$ ; ( $\lambda_{100} = -90 \cdot 10^{-6}$  and  $\lambda_{111} = -1350 \cdot 10^{-6}$ ) [17]; are of our especial interest. We notice that, in the contrast to them, the giant-magnetostriction Galfenol is of a near-zero rhombohedral magnetostriction.

### 3. Field and current-driven domain-wall motion

#### 3.1. DW mobility

In order to characterize the efficiency of the field-driven DW propagation and of the current-driven DW propagation, we determine the relevant mobilities of the head-to-head  $\pi/2$  DW with micromagnetic simulations. In particular, the maximum velocity

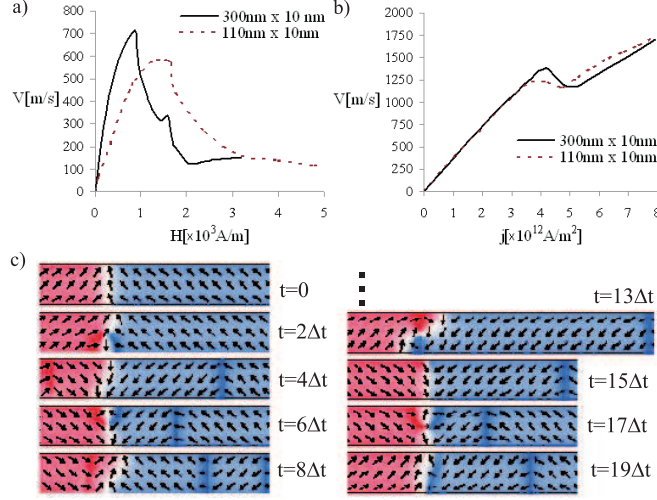


**Figure 2.** Top: the dependence of the velocity of the  $\pi/2$  head-to-head DW in the  $w \times \tau = 110 \times 10\text{nm}^2$  cross-section and  $w \times \tau = 300 \times 10\text{nm}^2$  cross-section nanostripes of the magnetite on the longitudinal magnetic field (a), and on the current intensity (b). Bottom: dynamical transformations of the propagating head-to-head DW in the  $w \times \tau = 300 \times 10\text{nm}^2$  cross-section nanostripe of the magnetite under the the longitudinal field  $H = 1670\text{A/m}$ . The time step is  $\Delta t = 3.0\text{ns}$ , the reference frame is connected to the DW moving right the picture.

of the viscous motion and the field intensity (current density) of the Walker breakdown are the characteristics which limit the applicability of DW-based devices. The velocity-field and velocity-current plots are shown in figure 2a and figure 2b, respectively, for the  $\text{Fe}_3\text{O}_4$  nanostripes of the widths  $w=110\text{nm}$  and  $w=300\text{nm}$  and of the thickness  $\tau=10\text{nm}$ . In the simulations (using the OOMMF package [24]), the cell size of the grid discretization is  $10\text{nm}$ , while the stripe length is  $30\mu\text{m}$ . In the plots, values of  $v(H)$  and  $v(j)$  are average velocities over  $15\mu\text{m}$  propagation distance. It should be stressed that this propagation distance is sufficient to determine  $v(H)$  in the considered range of the magnetic field and to determine  $v(j)$  in the regime of the viscous motion (below the critical current of the Walker breakdown). However, in the regime of turbulent motion (above the Walker breakdown), the propagation distance of  $15\mu\text{m}$  is insufficient to evaluate  $v(j)$  as an average over many cycles of DW transformations since the relevant propagation time is shorter than the period of the dynamical transformations of the DW. Therefore, the plotted in figure 2b  $v(j)$  curves do not resemble typical shape on the right-hand side of the local maximum (the Walker-breakdown peak) [25, 26]. On the other hand, for a reason discussed below (the fast Joule heating), there is no sense of simulating the DW motion on a wider time scale than the present one.

For the purpose of analyzing the plotted data, a simple 1D model of the field and current induced motion of the head-to-head (tail-to-tail)  $\pi/2$  DW is formulated in Appendix A. According to our analytical model, in the viscous-motion regime, the DW velocity depends on the intensity of the external field via the Walker-like formula  $v(H) = \gamma\mu_0\Delta H/\alpha$ , where the DW width corresponds to the exchange length of the crystalline anisotropy  $\Delta \approx \sqrt{-A/K_1}$ . Here,  $\gamma$  denotes the gyromagnetic factor,  $\mu_0$  the vacuum permeability,  $\alpha$  the Gilbert damping constant,  $A$  the exchange stiffness.

Basing on a 2D model of reference [9], the estimated in Appendix A width of the  $\pi/2$  DW has been renormalized by the factor of two;  $\Delta \approx 2\sqrt{-A/K_1}$  which leads to  $\Delta \approx 66\text{nm}$  for  $\text{Fe}_3\text{O}_4$ , and the DW mobility  $v(H)/H = \gamma\mu_0\Delta/\alpha = 1.04\text{m}^2/\text{As}$ . This value coincides with the mobility determined from figure 2a for the  $\pi/2$  DW in the aspect-ratio  $w/\tau = 30$  nanostripe. For the nanostripe of  $w/\tau = 11$ , we have established  $v(H)/H \approx 0.55\text{m}^2/\text{As}$ . Thus, the mobility of the  $\pi/2$  DWs in the  $\text{Fe}_3\text{O}_4$  nanostripes is found to be at least two times higher than estimated and measured in reference [26] for the vortex DWs in the Py nanostripes of the aspect ratio  $w/\tau = 10 \div 25$ ;  $v_{Py}(H)/H \approx 0.2 \div 0.3\text{m}^2/\text{As}$ , (here and below, the parameters of the Py systems are indexed with the relevant superscript). Moreover, for the stripes of similar aspect ratio, the Walker breakdown fields in the magnetite structures are larger than in the Py structures. In the consequence, the maximum velocity of the field-driven viscous motion of the  $\pi/2$  DW significantly exceeds that of the vortex DW in the Py nanostripes.

Similar to the  $\pi$  DW in the Permalloy, the head-to-head  $\pi/2$  DW undergoes a series of transformations into the vortex or/and antivortex DW above the Walker breakdown. There is characteristic peak in the field dependence of the DW velocity above the Walker breakdown that is well seen in  $v(H)$  plot for the nanostripe of the 300nm width (centered at the field value  $H \approx 1.5 \cdot 10^3\text{A/m}$ ) in figure 2a. It is accompanied by a transition between regimes of oscillatory and chaotic dynamical transformations of the DW following the nomenclature of reference [27], where similar peak has been found for  $\pi$  DWs in Py nanostripes. The transformation of the  $\pi/2$  DW into the antivortex DW is accompanied by the creation of two head-to-tail  $\pi/2$  DWs on both sides of the head-to-head DW [see the magnetization snapshots for  $0 \leq t \leq 8 \cdot 3\text{ns}$  in figure 2c], whereas, the transformation into the vortex DW and backward into the  $\pi/2$  DWs takes place during the passage of the head-to-head DW through a head-to-tail DW [see the magnetization snapshots for  $8 \cdot 3\text{ns} \leq t \leq 15 \cdot 3\text{ns}$  in figure 2c].

Within the 1D model of Appendix A, the velocity of the current-driven viscous propagation of the head-to-head (tail-to-tail)  $\pi/2$  DW is dependent of the current intensity following  $v(j) = \beta\eta j/\alpha$ . Here,  $\eta$  is the constant of the STT strength;  $\eta = Pg\mu_B/2eM$ , where,  $P$ ,  $g$ ,  $\mu_B$ , and  $e$  denote the spin polarization, the Lande factor, the Bohr magneton, and the electron charge, respectively [26]. In the simulations of the  $\text{Fe}_3\text{O}_4$  nanostripes;  $P = 0.94$ , thus,  $\eta = 1.9 \cdot 10^{-10}\text{m}^3/\text{C}$ , [28]. The ratio  $\beta/\alpha$  determines the non-adiabaticity of the STT in the LLG equation [29]. Assuming the corresponding non-adiabaticity indicator in the LL equation to be equal to one, we take  $\beta/\alpha = 2$ , (see [30]). Let us mention that, using the  $\pi$  DWs in Py nanostripes (the polarization  $P_{Py} = 0.5$ , the saturation magnetization  $M_{Py} = 8.6 \cdot 10^5\text{A/m}$ ), the relation  $\beta_{Py}/\alpha_{Py} = 2$  has been verified via measuring the DW velocity-to-current ratio  $v_{Py}(j)/j = 0.73 \cdot 10^{-10}\text{m}^3/\text{C}$ , [31].

We emphasize that current-related mobility of the head-to-head  $\pi/2$  DWs in the magnetite nanostripe;  $v(j)/j$  is higher for the magnetite nanostripe than for the head-to-head  $\pi$  DWs in the Py nanostripe, (because of higher spin polarization and lower saturation magnetization). Also, the breakdown current of the  $\pi/2$  DW in the magnetite (the critical current of the transition between viscous and turbulent motion regimes) is at least twice the breakdown current for the vortex DW in the Py nanostripe [31]. Therefore, the velocity of the simulated current-driven propagation of the  $\pi/2$  DW is as high as  $1100\text{m/s}$  for the current density of  $3 \cdot 10^{12}\text{A/m}^2$ . It significantly exceeds the highest reported velocity of the DW in a sandwiched (triple-

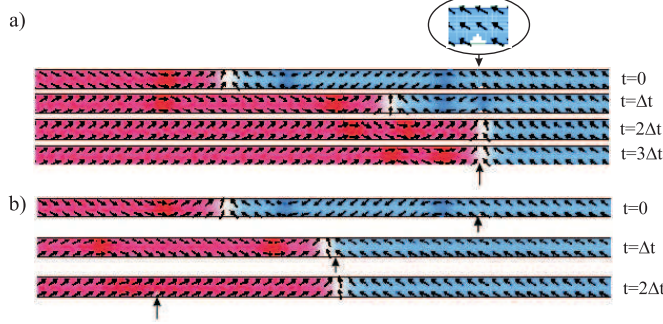


**Figure 3.** The current-driven motion of the  $\pi/2$ -DW in the presence of a pinning site at the lower edge of the  $\text{Fe}_3\text{O}_4$  stripe of the  $w \times \tau = 110 \times 10 \text{ nm}^2$  cross-section. The current densities are  $j = 1 \cdot 10^{12} \text{ A/m}^2$  (a), and  $j = 1.5 \cdot 10^{12} \text{ A/m}^2$  (b). The time step is  $\Delta t = 3.2 \text{ ns}$ . In b) the reference frame is moving relative to the pinning site.

layer) nanostripe;  $750 \text{ m/s}$ , that has been induced with similar value of the current density [32]. However, unlike the sandwiched nanostripe of reference [32] (an artificial antiferromagnet), our ferromagnetic system enables the field-driven propagation of the DW as well! Moreover, following the present simulations, under currents exceeding the breakdown value, on a certain time scale that is shorter than the time of the dynamical transformation of the DW, (thus, the DW motion is thought of to be almost viscous), the velocity of the head-to-head  $\pi/2$  DWs can be even higher than  $1100 \text{ m/s}$ .

The field-driven and current-driven motions of the head-to-head (tail-to-tail)  $\pi/2$  DWs are different in another aspect than previously mentioned as well. Unlike the current, the longitudinal external field does not drive the head-to-tail  $\pi/2$  DWs to move. It is because the propagation of the head-to-tail DW is not accompanied by any change of the Zeeman energy in itself while the Zeeman energy changes during shrinking or expanding the superdomains (the propagation of the head-to-head and tail-to-tail DWs). In the consequence, the head-to-head  $\pi/2$  DW propagates pushing one or two head-to-tail DWs. Any next head-to-tail DW that appears on the way of the complex of the three  $\pi/2$  DWs is annihilated during the collision, which is accompanied by a reduction of the complex to a pair of the DWs (one of the head-to-head type and one of the head-to-tail type).

### 3.2. DW depinning and issue of thermal stability

The issue to address is the strength of the pinning of the head-to-head (tail-to-tail) DW by stripe constrictions. The periodically distributed constrictions are considered to be pinning centers that stabilize the DW position in the racetrack counteracting mutual interactions between the DWs. We simulate the depinning of the DW from an artificially created (at one of the stripe edges) notch. The depth of the notch is  $3/10$  of the stripe width while its shape is triangular. Remark that, in usual simulations of the current-driven motion of the DW, the depth of the notch is limited by the assumption of the uniform density of the current (the parameter of the STT is taken to be constant). That assumption could be contested when a variation of the stripe cross-section was large (the constriction of the stripe was very narrow).

According to figure 3 and figure 4, the courses of the pinning/depinning processes are dependent on the orientation of the pinning-site triangle relative to the directions



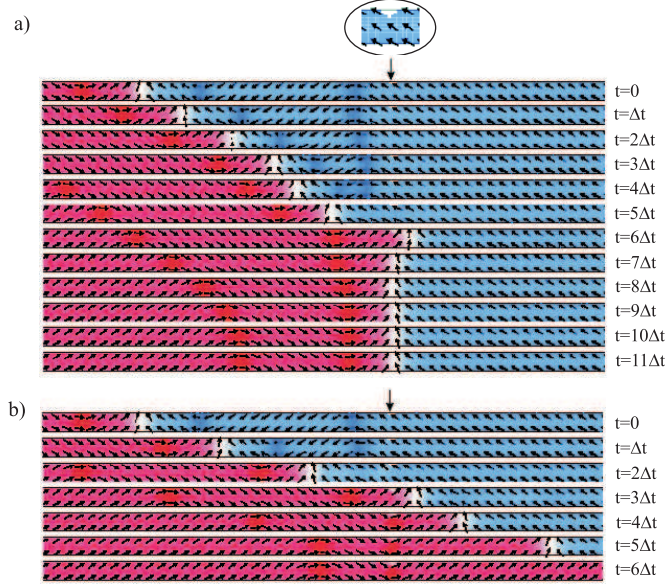


**Figure 4.** The current-driven motion of the  $\pi/2$ -DW in the presence of a pinning site at the upper edge of the  $\text{Fe}_3\text{O}_4$  stripe of the  $w \times \tau = 110 \times 10\text{nm}^2$  cross-section. The current densities are  $j = 2.5 \cdot 10^{11}\text{A/m}^2$  (a), and  $j = 5 \cdot 10^{11}\text{A/m}^2$  (b). The time step is  $\Delta t = 3.2\text{ns}$ .

of the magnetization of the closest domains. The strongest pinning is present when the domains are magnetized parallel to the border of the notch, and this observation concerns the head-to-head (tail-to-tail)  $\pi/2$  DWs as well as the head-to-tail  $\pi/2$  DWs. The density of the depinning current for the head-to-head  $\pi/2$  DW in  $w \times \tau = 110\text{nm} \times 10\text{nm}$  magnetite stripe appeared not to exceed  $1.5 \cdot 10^{12}\text{A/m}^2$ , which is several times higher value than achievable with PMA nanostripes while lower than the depinning current of the transverse DWs in the Py nanostripes of similar cross sections with similar notches [3]. Unfortunately, details of the notch shape are not standardized. A quite independent of those details indicator of the efficiency of the current-driven depinning is the ratio of the depinning current  $j_p$  to the depinning field  $H_p$ .

For the given depth of the notch, we have confirmed the theoretical relation  $j_p = \alpha\mu H_p / \beta\eta$  with the simulations. Here  $\mu \equiv v(H)/H$  denotes the DW mobility. For instance, the ratio  $j_p/H_p = 1.46 \cdot 10^{12}\text{Am}^{-2}/955\text{Am}^{-1} = 1.5\text{nm}^{-1}$  has been obtained from the simulations of  $w \times \tau = 110\text{nm} \times 10\text{nm}$  magnetite nanostripe with the geometry of figure 3 (the notch at the lower edge, the DW magnetized upward the stripe plane). It coincides with the theoretical value  $\alpha\mu/\beta\eta = 0.55\text{m}^2\text{C}^{-1}/2 \cdot 1.9 \cdot 10^{-10}\text{m}^3\text{C}^{-1} = 1.5\text{nm}^{-1}$ . Following reference [33], the maximum of the relevant ratio for the transverse DWs in the  $w \times \tau = 300\text{nm} \times 10\text{nm}$  Py nanostripe takes the value of  $j_p^{Py}/H_p^{Py} = 3 \cdot 10^{12}\text{Am}^{-2}/3500\text{Am}^{-1} = 0.86\text{nm}^{-1}$ . Extrapolating this ratio to the nanostripe of  $100\text{nm}$  width (dividing it by three) leads to five times smaller value than for the head-to-head  $\pi/2$  DW in the magnetite nanostripe ( $j_p/H_p = 5j_p^{Py}/H_p^{Py}$ ). Notice that the low efficiency of the current-induced depinning (high  $j_p/H_p$  ratio) is not a disadvantage in itself. While the depinning current cannot be largely reduced with the magnetite nanostripe compared to that of the Py nanostripe, the depinning

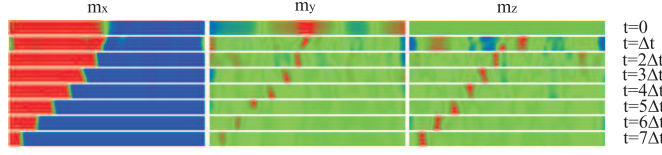


**Figure 5.** The stress-driven motion of the head-to-head DW in  $\text{Fe}_3\text{O}_4$  nanostripe of the  $w \times \tau = 100 \times 10 \text{ nm}^2$  cross-section. The stress components are  $\sigma_x = 0.6 \text{ GPa}$ ,  $\sigma_y = 2.4 \text{ GPa}$ ,  $\sigma_z = 0$ . The time step  $\Delta t = 0.5 \text{ ns}$ .

field can be and it is found smaller than the Walker-breakdown value in the magnetite nanostripes. This enables the field-only driven viscous motion of the  $\pi/2$  DW in the presence of the notches. In the case of the  $\pi$  DWs, such a motion was impossible in the Py nanostripes nor with the PMA nanostripes.

We note that, for a head-to-head DW magnetized upward the nanostripe, the ratio of the depinning current and the depinning field for the nanostripe with the notch at upper edge (figure 4) is similar to that for the lower-edge patterned nanostripe of figure 3. However, in the former case, the depinning current is only  $j_p = 0.44 \cdot 10^{12} \text{ A m}^{-2}$ . The strength of the mutual interactions of the head-to-head and tail-to-tail  $\pi/2$  DWs requires a complex study (which is beyond the scope of the paper) in order to assess the minimal pinning field necessary. In particular, the mediating role of the structure of the head-to-tail DWs (whose period is scalable with stripe thickness) is to be determined.

In order to determine the pace of the temperature increase due to the Joule heating, we apply the formula  $dT/dt = j^2/\sigma C\rho$ , where,  $\sigma$  denotes the electrical conductivity,  $C$  denotes the specific heat capacity, while  $\rho$  denotes the mass density. For  $\text{Fe}_3\text{O}_4$  nanostripe, in the presence of the current of the density  $j = 10^{12} \text{ A m}^{-2}$ , ( $\sigma = 1.0 \cdot 10^4 \text{ } \Omega\text{m}$ ,  $C = 0.67 \text{ J/gK}$ ,  $\rho = 5.0 \cdot 10^3 \text{ kg/m}^3$ ) [34, 35], one estimates  $dT/dt = 3.0 \cdot 10^4 \text{ K/ns}$ . The last value is significantly higher than for the Py nanostripe with the current of the same density [36, 37];  $dT/dt = 91 \text{ K/ns}$ , which is due to small electrical conductivity of the magnetite compared to Py. Notice that the Curie temperatures of Py and  $\text{Fe}_3\text{O}_4$  are similar,  $T_c \approx 850 \text{ K}$ . Any hope for slowing down the Joule heating of the magnetite nanostripe via material modifications (e.g. doping) in the direction of reduction of the electrical resistivity is weak since  $\text{Fe}_3\text{O}_4$  is the material of the lowest resistivity among all spinels. Hence, the limitation on the time length of the current pulses usable to drive the DW propagation in the magnetite nanostripes ( $\sim 10 \text{ ps}$ ) is much stronger than for the Py stripes ( $\sim 1 \text{ ns}$ ). However, the spatial distances between the neighboring head-to-head and tail-to-tail  $\pi/2$  DWs can be substantially reduced compared to the minimum spacing of the transverse/vortex DWs in the soft-magnetic nanostripes while the velocities of the DWs of the former type are an order of magnitude higher than those of the vortex DWs. Therefore, operating the  $\text{Fe}_3\text{O}_4$  structures with ultra-short current pulses can be as efficient as operating the Py structures with the ns pulses.

#### 4. Stress-driven domain-wall motion

We verify whether the stress application is an efficient alternative to the field application when driving of the DW propagation. With this purpose, we have performed the simulations of the stress-driven motion of the DW for the magnetite

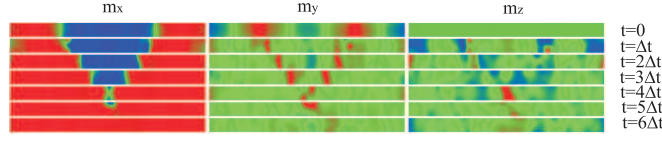


**Figure 6.** The mutual annihilation of two DWs (one head-to-head DW and one tail-to-tail DW) via the stress-driven collision in  $\text{Fe}_3\text{O}_4$  nanostripe of the  $w \times \tau = 100 \times 10\text{nm}^2$  cross-section, ( $\sigma_x = 0.5\text{GPa}$ ,  $\sigma_y = 2.0\text{GPa}$ ,  $\sigma_z = 0$ ,  $\Delta t = 1\text{ns}$ ). A transverse field of  $30\text{mT}$  is applied in the direction  $(0,1,-1)$ .

stripe of the width  $w = 100\text{nm}$  and thickness  $\tau = 10\text{nm}$ . The effects of the constant stress are easy to simulate with the MAGPAR package that we have utilized [38]. The direction of the (in-the-plane) stress vector is taken with  $\sigma_x/\sigma_y = 1/4$ ,  $\sigma_z = 0$ , where  $x$  corresponds to the long axis of the stripe while  $z$  axis coincides with the out-of-plane direction. The stripe length is  $1.5\mu\text{m}$ .

With the snapshots in figure 5, it is seen that the dynamics of the DW consists of two stages. Upon switching the stress on, the ferromagnetic domains undergo an almost instant reorientation because the tetragonal magnetostriction creates novel easy directions. It forces the transition of the head-to-head (tail-to-tail)  $\pi/2$  DW into the  $\pi$ -like DW within  $1\text{ns}$  approximately. In fact, the stress-induced anisotropy due to the tetragonal magnetostriction is two-axial while both easy (in-the-plane) directions are slightly deviated from the long axis of the stripe. At the second stage of the simulations, the internal field due to the rhombohedral magnetostriction drives the resulting  $\pi$ -like DW to propagate along the wire. The propagation takes place under sufficiently high total stress  $\sigma \equiv |\sigma| \geq 0.6\sqrt{17}\text{GPa}$ . However, this lower bound on the motion-driving stress is not any fundamental value while the minimum stress changes with the simulation conditions (with the stripe length for instance). Its presence can be explained by changing the preference of the system in terms of the stabilization of the  $\pi$  DW or another head-to-head DW (a  $\pi - \epsilon\pi$  DW, where  $\epsilon \ll 1$ ) under the stress. The later structure propagates while the former is static as mentioned in Sec. II. Turning on the stress in presence of a weak perpendicular magnetic field ensures the desired noncollinearity of the magnetization to be present. In particular, in the presence of a transverse in-the-plane field of  $20\text{mT}$ , the simulated DW propagates under the (subcritical) stress of  $\sigma = 0.5\sqrt{17}\text{GPa}$ .

Notice that the stabilizing DWs are not in-the-plane magnetized while they are intermediate between the Bloch-like and Neel-like DWs. The stress-induced motion is almost viscous, however, minor oscillations of the DW structure are seen.

The estimations based on the formulae of Appendix B, for the stress components  $\sigma_x = 0.6\text{GPa}$ ,  $\sigma_y = 2.4\text{GPa}$ ,  $\sigma_z = 0$  applied to the magnetite nanostripe (figure 5), lead to the DW width  $\Delta \approx 26\text{nm}$  for  $\cos(\varphi) = 1/10$  (an almost Bloch DW). The velocity of the viscous propagation with dependence on the stress is given by formula (B.3). It leads, via  $\mu_\sigma = 270 \cdot 10^3\text{m/sGPa}$ , for the above values of the stress components, to the DW velocity  $1600\text{m/s}$  that significantly overestimates the simulation result:  $210\text{m/s}$  (in the relevant figure 5, the stripe length is  $1.5\mu\text{m}$ ). The discrepancy is not a surprise, however, since the DW motion is not fully turbulent (slow) nor purely viscous (fast), as seen from figure 5. The intermediate (oscillatory) character of the motion is expected to be accompanied by a decrease of the average velocity compared to the estimated value.

In figure 6, we demonstrate (by means of the micromagnetic simulations) the stress-induced collision of the head-to-head and tail-to-tail  $\pi/2$  DWs and the possibility of annihilating the DW pairs. Because of an instability of the direction of the DW magnetization, a weak transverse (to the long axis) field of 30mT is applied and it is deviated from the stripe plane by  $\pi/4$  angle. Upon that stabilization, projections of the magnetizations of the colliding DWs are directed similar while the DW motion is viscous. Therefore, the expected result of the collision is mutual annihilation of the DWs following a general rule; the parallel (antiparallel) magnetized ferromagnetic DWs attract (repulse) [39, 40]. Our simulations confirm this expectation (figure 6).

Addressing the way of application of the stress to the nanostripe, we mention the strain-mediated magnetoelectric effect in the multiferroic laminates. For instance, the magnetoelectricity of  $\text{Fe}_3\text{O}_4/\text{PZN-PT}$  and  $\text{Fe}_3\text{O}_4/\text{PMN-PT}$  is one of the strongest reported to date [41]. A rough estimation based on the data of reference [42] shows sub-GPa in-the-plane stress to be induced in a quite thick (sub- $\mu\text{m}$ ) structural magnetite layer upon the application of the electric field of 6kV/cm in the PZN-PT substrate. Moreover, increasing the stress in the magnetic layer via engineering the interface of the magnetoelectric composite is the subject of successive studies (e.g. [43]). Therefore, we believe the desired values of the stress to be achievable with a simple voltage application.

## 5. Conclusions

We have analyzed the field, current, and stress driven propagation of the  $\pi/2$  DWs in the nanowires (nanostripes) created of cubic-anisotropy ferromagnetic materials. with relevance to the potential application of those textures to the DW racetrack memory. The  $\pi/2$  DWs are much narrower than the transverse DWs in the soft-magnetic nanowires of similar cross-sections which enables the recording with a bit density comparable to that of the PMA nanowires. In spite of the small width of the  $\pi/2$  DWs, the predicted velocities of the field-driven viscous motion of the  $\pi/2$  DWs in the magnetite nanostripes are higher than achievable for  $\pi$  DWs in the Py nanostripes. It is because of large values of the critical field of the Walker breakdown in the magnetite nanostructures. Let us recall that such a viscous field-driven motion is not achievable with the single-layer PMA nanowires.

The current-driven propagation of the  $\pi/2$  DWs can be even faster than the fastest reported propagation of the chiral (Bloch) DWs in multi-layered nanowires with the PMA [32]. However, unlike for  $\pi$  DW in the PMA nanowires, designing the racetrack for the  $\pi/2$  DWs, there is no need to involve other mechanisms of the propagation driving with current than the direct STT. The conservation of the global chirality of the system of many  $\pi/2$  DWs does not play any role in its positioning.

The possibility of the stress-driven propagation of the DWs arises due to the anisotropy of the magnetostriction. We have demonstrated by means of the micromagnetic simulation the stress-induced collision of the DWs that results, under some stabilizing transverse field, in the annihilation of the DW pair. Hence, the stress application is found to be an alternative to using the longitudinal magnetic field when driving the domain magnetization reversal.

The promising cubic-anisotropy material considered is the magnetite. First, because of a relatively low saturation magnetization (a weak shape anisotropy) and a strong cubic anisotropy, which enables the creation of the  $\pi/2$  DWs. Second, because of large ratio of the rhombohedral magnetostriction constant to the tetragonal

magnetostriction constant, which enables high-speed propagation of the DWs driven by the stress. Unfortunately, because of large electrical resistivity of the magnetite (the resistivity of the ferrites is two or three orders of magnitude larger than the resistivity of the Permalloy), the Joule heating remains a crucial problem in the racetrack design. However, small lengths of the domains and large velocities of the DWs enable as efficient current-driven positioning of the many-domain record as achievable with the Py-based racetracks, albeit using much shorter current pulses.

Finally, we notice that the material parameters of the Terfenol-D seem to make it the most relevant material to manufacture the racetrack of the  $\pi/2$  DWs. It is of a very strong cubic anisotropy (of a negative value of the  $K_1$  constant as desired) and of an extremely strong rhombohedral magnetostriction. A relatively small saturation magnetization (a weak shape anisotropy compared to the crystalline anisotropy) leads to the formation of very narrow  $\pi/2$  DWs in a wide range of thicknesses of the nanostripes (they are stable for up to 40nm-thick stripes). The electrical resistivity of the Terfenol-D is only  $6.0 \cdot 10^{-5} \Omega \text{cm}$  while the specific heat capacity and the mass density are comparable to those of the magnetite and Py, thus, the Joule heating is slow [44]. A quite big (estimated) value of the Gilbert damping constant of the Terfenol-D is a potential disadvantage that limits the DW velocity however. On the other hand, the brittleness of the Terfenol-D makes it difficult to process to the nanoscale, (while the nanotechnology of the magnetite is advanced [45]).

## Appendix A. Field (current) driven dynamics of $\pi/2$ DW in 1D

We treat a model of the  $\pi/2$  DW motion analytically solving the LLG equation

$$-\frac{\partial \mathbf{m}}{\partial t} = \gamma \mathbf{m} \times \left( \mathbf{B}_{eff} - \frac{\alpha}{M} \frac{\partial \mathbf{m}}{\partial t} + \frac{\eta j}{\gamma M^2} \mathbf{m} \times \frac{\partial \mathbf{m}}{\partial x} + \frac{\beta \eta j}{\gamma M} \frac{\partial \mathbf{m}}{\partial x} \right) \quad (\text{A.1})$$

in 1D. Here,  $B_{eff}^{(i)} \equiv -\delta \mathcal{H} / \delta m_i$  while

$$\mathcal{H} \equiv A \left( \frac{\partial \mathbf{m}}{\partial x} \right)^2 - \frac{K_{\parallel}}{M^2} (\mathbf{m} \cdot \hat{i})^2 + \frac{K_{\perp}}{M^2} (\mathbf{m} \cdot \hat{k})^2 - \mathbf{m} \cdot \mathbf{B} + \mathcal{H}_{ca} + \mathcal{H}_{me} \quad (\text{A.2})$$

Here,  $\hat{i} \equiv (1, 0, 0)$ ,  $\hat{k} \equiv (0, 0, 1)$ , (the stripe is directed along the  $x$  axis while  $z$  axis is normal to the stripe plane),  $\gamma$  denotes the gyromagnetic factor,  $A$  denotes the exchange stiffness. The longitudinal external field  $H$  is defined via  $\mathbf{B} = (\mu_0 H, 0, 0)$ . The effective easy-axis ( $K_{\parallel}$ ) and easy-plane ( $K_{\perp}$ ) anisotropies are of the shape (magnetostatic) origin. The (cubic) crystalline anisotropy and the magnetoelastic coupling are included with the  $\mathcal{H}_{ca}$ ,  $\mathcal{H}_{me}$  terms of the Hamiltonian, respectively. The constants of the normal and anomalous STT are denoted with  $\eta$  and  $\eta \cdot \beta$ , correspondingly, while  $j$  denotes the density of the electric current.

Parametrizing the magnetization with angles;  $\mathbf{m} = M[\cos(\theta), \sin(\theta) \cos(\varphi), \sin(\theta) \sin(\varphi)]$ , one describes a  $\pi/2$  DW texture with  $\theta = \pi/4 + \arctan(b/a)$ ,  $b = 1$ ,  $a = \exp\{[x - q(t)]/\Delta(t)\}$ . That ansatz for solving the equation (A.1) is a modified (via including the dependence of  $q$  and  $\Delta$  on the time) static solution to the LLG equation [9]. Inserting the ansatz into (A.1), we notice that  $a/\sqrt{(a^2 + b^2)} = \cos(\theta - \pi/4)$ ,  $b/\sqrt{(a^2 + b^2)} = \sin(\theta - \pi/4)$ , thus,  $\sin(\theta) = (a + b)/\sqrt{2(a^2 + b^2)}$ ,  $\cos(\theta) = (a - b)/\sqrt{2(a^2 + b^2)}$ . For  $\varphi = 0$  (the in-the-plane ordering), and  $\dot{\Delta} = 0$  (a sufficiently-long time upon switching the field or current on [29, 30]), one arrives at the system of the equations

$$\frac{1}{\Delta} (\dot{q} + \eta j) \frac{ab}{\sqrt{a^2 + b^2}} + \alpha \dot{\varphi} \frac{(a + b)}{\sqrt{2}} = 0,$$

$$\left(\frac{2\gamma A}{\Delta^2 M} + \frac{2\gamma K_1}{M}\right) \frac{ab(b^2 - a^2)}{(a^2 + b^2)^{3/2}} - \frac{\gamma K_{\parallel}}{M} \frac{b^2 - a^2}{\sqrt{a^2 + b^2}} - (\gamma\mu_0 H + \dot{\varphi}) \frac{(a+b)}{\sqrt{2}} + \left(\frac{\alpha}{\Delta} \dot{q} + \frac{\beta\eta j}{\Delta}\right) \frac{ab}{\sqrt{a^2 + b^2}} = 0. \quad (\text{A.3})$$

In the center of the DW [for  $x = q(t)$ ], thus, for  $a = b = 1$ , these equations simplify to

$$\begin{aligned} \frac{\dot{q} + \eta j}{2\Delta} + \alpha \dot{\varphi} &= 0, \\ \gamma\mu_0 H + \dot{\varphi} - \frac{\alpha \dot{q} + \beta\eta j}{2\Delta} &= 0. \end{aligned} \quad (\text{A.4})$$

A rough estimate of the width of the DW using (A.3) leads to  $\Delta = \sqrt{A/(K_{\parallel} - K_1)}$ , where  $|K_1| \gg 1/10\mu_0 M^2 > K_{\parallel}$  for the aspect ratio  $w/t \approx 10$ , (estimation details follow reference [26]).

The first of equations (A.3) and the first of equations (A.4) become irrelevant to the description of the viscous DW motion since they originate from the dynamical equation of the out-of-plane magnetization component  $m_z$ . One removes them [25], thus, finding  $\dot{q} = (-\beta\eta j + \gamma\Delta H)/\alpha$ .

## Appendix B. Stress-driven dynamics of DW in 1D

We consider the head-to-head or tail-to-tail DW under an in-the-plane directed and sufficiently-strong external stress. According to the simulation of section IV, the domains which are magnetized in the  $(1, \pm 1, 0)$  directions in the absence of the stress rapidly remagnetize onto the long axis of the stripe upon switching the stress on. Thus, the head-to-tail DWs disappear while the head-to-head (tail-to-tail)  $\pi/2$  DWs transform into  $\pi$  DWs. The domain remagnetization is not complete however, while the magnetization direction is weakly deviated from the longitudinal one. That enables the creation of the longitudinal field inside the domains with the stress, thus, driving the DW motion can be explained with minimizing the energy via shrinking (developing) the domains magnetized almost antiparallel (parallel) to the field (similar to minimizing the Zeeman energy via the DW propagation). Additionally, an in-the-plane anisotropy is created with the stress, which influences the DW width.

In order to model the stress-induced dynamics of the  $\pi$ - $\epsilon$  DW in the limit  $\epsilon \rightarrow 0^+$ , we apply the standard ansatz  $\theta = 2\arctan(b/a)$ ,  $b = 1$ ,  $a = \exp\{[x - q(t)]/\Delta(t)\}$  that is used to describe the motion of the  $\pi$  DW in the wires. Notice that  $\sin(\theta) = 2ab/(a^2 + b^2)$ ,  $\cos(\theta) = (a^2 - b^2)/(a^2 + b^2)$ . We consider the long-term dynamics,  $\dot{\Delta} = 0$ , in the absence of the external magnetic field and electric current. The substitution of the ansatz into the LLG system, for  $|\varphi| \ll \pi/2$ , leads to

$$\begin{aligned} \frac{\dot{q}}{\Delta} + \alpha \dot{\varphi} &= 0, \\ -\dot{\varphi} + \frac{\alpha}{\Delta} \dot{q} + \left[ -\frac{2\gamma[K_{\parallel} + K_{\perp}\sin^2(\varphi)]}{M} - \frac{2\gamma K_1}{M} \frac{(a^2 - b^2)^2 - 4a^2b^2}{(a^2 + b^2)^2} + \frac{2\gamma A}{\Delta^2 M} \right. \\ &\quad \left. + \frac{3\gamma\lambda_{100}\sigma\cos(\varphi)}{M}(\gamma_2^2 - \gamma_1^2) \right] \frac{b^2 - a^2}{a^2 + b^2} - \frac{3\gamma\lambda_{111}\sigma\gamma_1\gamma_2}{M} \frac{(a^2 - b^2)^2 - 4a^2b^2\cos^2(\varphi)}{2ab(a^2 + b^2)} = 0, \end{aligned} \quad (\text{B.1})$$

where  $\gamma_1 \equiv \sigma_x/\sigma$ ,  $\gamma_2 \equiv \sigma_y/\sigma$ , and  $\sigma \equiv |\sigma|$ . In the center of the DW,  $a = b = 1$ . Assuming the range of stresses  $K_{\parallel} + K_{\perp}\sin^2(\varphi) \ll -K_1 - 3\lambda_{100}\sigma(\gamma_2^2 - \gamma_1^2)\cos(\varphi)$ , the

second equation of (B.1) leads to

$$\Delta = \sqrt{\frac{2A}{-2K_1 - 3\lambda_{100}\sigma(\gamma_2^2 - \gamma_1^2)\cos(\varphi)}}. \quad (\text{B.2})$$

The last relation limits the range of  $\varphi$  angle to  $\cos(\varphi) > 0$ , thus, the rotation of the DW magnetization, if takes place, is not stationary while oscillatory. We evaluate the velocity of the stress-driven (viscous) motion of the DW

$$\begin{aligned} \dot{q} &= \mu_\sigma \cos^2(\varphi) \gamma_1 \gamma_2 \sigma, \\ \mu_\sigma &\equiv \frac{3\gamma\lambda_{111}\Delta}{M\alpha}. \end{aligned} \quad (\text{B.3})$$

Following (B.3), since  $\pi$  DWs are completely out-of-the-plane magnetized, ( $\varphi = \pm\pi/2$  in the center of the  $\pi$  DW), they cannot be driven by the stress, whereas,  $\pi - \epsilon$  DWs which separate slightly noncollinear domains can, ( $\varphi \neq \pm\pi/2$  in the center of such a DW).

## References

- [1] Parkin S S P, Hayashi M, Thomas L 2008 *Magnetic domain-wall racetrack memory*, Science **320** 190
- [2] Allwood D A, et al. 2005 *Magnetic domain-wall logic* Science **309** 1688
- [3] Thomas L, et al. 2011 *Racetrack Memory: a high-performance, low-cost, non-volatile memory based on magnetic domain walls* Proc. IDEM11, 535
- [4] Zhang Y, Zhao W S, Klein J-O, Chappert C, Ravelosona D 2014 *Current induced perpendicular magnetic anisotropy racetrack memory with magnetic field assistance* Appl. Phys. Lett. **104** 032409
- [5] Parkin S, Yang S-H 2015 *Memory on the racetrack*, Nature Nanotech. **10** 195
- [6] Metaxas P J, et al. 2007 *Creep and Flow Regimes of Magnetic Domain-Wall Motion in Ultrathin Pt/Co/Pt Films with Perpendicular Anisotropy* Phys. Rev. Lett. **99** 217208
- [7] Martinez E 2012, *Static Properties and Current-Driven Dynamics of Domain Walls in Perpendicular Magnetocrystalline Anisotropy Nanostrips with Rectangular Cross-Section* Adv. Cond. Matt. Phys. **2012** 954196
- [8] Emori S, Bauer U, Ahn S-M, Martinez E, Beach G S D 2013 *Current-driven dynamics of chiral ferromagnetic domain walls* Nature Mater. **12** 611
- [9] Janutka A, Gawronski P 2014 *Domain walls in nanostripes of cubic-anisotropy ferromagnetic materials* IEEE Trans. Magn. **50** 1100404
- [10] Kronmüller H, Fähnle M 2003 *Micromagnetism and the Microstructure of Ferromagnetic Solids* Cambridge Univ. Press, Cambridge
- [11] Galt J K 1954 *Motion of Individual Domain Walls in Nickel-Iron Ferrite*, Bell Syst. Tech. J. **33** 1023
- [12] Bozorth R M, Tilden E F, Williams A J 1955 *Anisotropy and Magnetostriction of Some Ferrites* Phys. Rev. **99** 1788
- [13] Brandlmaier A, et al. 2008 *In situ manipulation of magnetic anisotropy in magnetite thin films* Phys. Rev. B **77** 104445
- [14] Nagata M, et al. 2014 *Ferromagnetic Resonance in Magnetite Thin Films* IEEE Trans. Magn. **50** 1400203
- [15] Sofin R G S, Arora S K, Shvets I V 2011 *Positive antiphase boundary domain wall magnetoresistance in  $\text{Fe}_3\text{O}_4(110)$  heteroepitaxial films* **83**, 134436
- [16] T Schemme, et al. 2015 *Magnetic anisotropy related to strain and thickness of ultrathin iron oxide grown on  $\text{MgO}(001)$*  Mater. Res. Express **2** 016101,  
T Schemme, et al. 2015 *Modifying magnetic properties of ultra-thin magnetite films by growth on Fe pre-covered  $\text{MgO}(001)$*  J. Appl. Phys. **118** 113904
- [17] de la Fuente C, et al. 2004 *Magnetocrystalline anisotropy in a (110)  $(\text{Tb}_{0.27}\text{Dy}_{0.73})\text{Fe}_2$  thin film* J Phys. D **16** 2959
- [18] Fashami M S, Roy K, Atulasimha J, Bandyopadhyay S 2011 *Magnetization dynamics, Bennett clocking and associated energy dissipation in multiferroic logic*, Nanotechnology **22** 155201

- [19] Fonin M 2011 *Formation of magnetic domains and domain walls in epitaxial  $\text{Fe}_3\text{O}_4(100)$  elements* J. Appl. Phys. **109** 07D315
- [20] Beach G S D, Knutson C, Tsoi M, Erskine J L 2007 *Field- and current-driven domain wall dynamics: An experimental picture* **310** 2038
- [21] Brintlinger T 2010 *In Situ Observation of Reversible Nanomagnetic Switching Induced by Electric Fields* **10** 1219
- [22] Parks D A, et al. 2012 *Non-volatile voltage control of magnetization and magnetic domain walls in magnetostrictive epitaxial thin films* Appl. Phys. Lett. **101**, 072402
- [23] Grossinger R, Sato Turtelli R, Mehmood N 2014 *Materials with high magnetostriction* IOP Conf. Series: Mater. Sci. and Eng. **60** 012002
- [24] [math.nist.gov/oommf/](http://math.nist.gov/oommf/)
- [25] Thiaville A, Nakatani Y, Miltat J, Suzuki Y 2005 *Micromagnetic understanding of current-driven domain wall motion in patterned nanowires* Europhys. Lett. **69** 990
- [26] Beach G S D, Tsoi M, Erskine J L 2008 *Current-induced domain wall motion* J Magn. Magn. Mat. **320** 1272
- [27] Lee J Y, Lee K S, Choi S, Guslienko K Y, Kim S K 2007 *Dynamic transformations of the internal structure of a moving domain wall in magnetic nanostripes*, Phys. Rev. B **76** 184408
- [28] Cespedes O, Clifford E, Coey J M D 2005 *Magnetoresistance of magnetite point contacts and nanoconstrictions* J. Appl. Phys. **97** 064305
- [29] Zhang S, Li Z 2004 *Roles of Nonequilibrium Conduction Electrons on the Magnetization Dynamics of Ferromagnets* Phys. Rev. Lett. **93** 127204
- [30] Tserkovnyak Y, Brataas A, Bauer G E W 2008 *Theory of current-driven magnetization dynamics in inhomogeneous ferromagnets* J Magn. Magn. Mat. **320** 1282
- [31] Hayashi M, et al. 2007 *Current Driven Domain Wall Velocities Exceeding the Spin Angular Momentum Transfer Rate in Permalloy Nanowires* Phys. Rev. Lett. **98** 037204
- [32] Yang S-H, Ryu K-S, Parkin S 2015 *Domain-wall velocities of up to  $750\text{ms}^{-1}$  driven by exchange-coupling torque in synthetic antiferromagnets* Nature Nanotech. **10** 221
- [33] Hayashi M, et al. 2006 *Dependence of Current and Field Driven Depinning of Domain Walls on Their Structure and Chirality in Permalloy Nanowires*, Phys. Rev. Lett. **97** 207205
- [34] Ziemniak S E, et al. 2007 *Magnetic contribution to heat capacity and entropy of nickel ferrite* J. Phys. Chem. Sol. **90** 1515
- [35] Naftalis N, et al. 2013 *Thickness dependence of the resistivity tensor in epitaxial magnetite thin films* J. Appl. Phys. **114** 043701
- [36] Fangohr H, et al. 2011 *Joule heating in nanowires* Phys. Rev. B **84** 054437
- [37] Counil G, et al. 2006 *Temperature Dependences of the Resistivity and the Ferromagnetic Resonance Linewidth in Permalloy Thin Films* IEEE Trans. Magn. **42** 3323
- [38] [www.magpar.net/](http://www.magpar.net/)
- [39] Janutka A 2013 *Complexes of Domain Walls in One-Dimensional Ferromagnets Near and Far from Phase Transition* Acta Phys. Pol. A **124** 23
- [40] Janutka A 2013 *Short-Range Interactions of Domain Walls in Ferromagnetic Nanostripes* IEEE Magn. Lett. **4** 4000304
- [41] Vaz C A F 2012 *Electric field control of magnetism in multiferroic heterostructures* J. Phys.: Condens. Matter **24** 333201
- [42] Liu M, et al. 2010 *Electrical tuning of magnetism in  $\text{Fe}_3\text{O}_4/\text{PZN-PT}$  multiferroic heterostructures derived by reactive magnetron sputtering* J. Appl. Phys. **107** 073916
- [43] Gueye M, Zighem F, Faurie D, Belmeguenai M, Mercone S 2014 *Optimization of indirect magnetoelectric effect in thin-film/substrate/piezoelectric-actuator heterostructure using polymer substrate* Appl. Phys. Lett. **105** 052411
- [44] Cook B A, et al. 2000 *Electrical and thermal properties of  $\text{Tb}_{0.3}\text{Dy}_{0.7}\text{Fe}_{2-x}$*  J. Appl. Phys. **87** 776
- [45] Eltschka M, et al. 2008 *Correlation between magnetic spin structure and the three-dimensional geometry in chemically synthesized nanoscale magnetite rings* Appl. Phys. Lett. **92**, 222508